J. Plasma Phys. (2024), *vol*. 90, 965900201
Published by Cambridge University Press

doi:10.1017/S0022377824000461

Proton acceleration from optically tailored high-density gas jet targets

A. Maitrallain[1],†, J.-R. Marquès[2], K. Bontemps[1], J. Bonvalet[3], E.F. Atukpor[1], V. Bagnoud[4], T. Carrière[3], F. Hannachi[1], J.L. Henares[5], J. Hornung[4], A. Huber[1], E. d'Humières[3], L. Lancia[2], P. Loiseau[6,7], P. Nicolaï[3], J. Santos[3], V. Tikhonchuk[3], B. Zielbauer[4] and M. Tarisien[1],†

[1]University of Bordeaux, CNRS, LP2I, UMR 5797, F-33170 Gradignan, France

[2]LULI, CNRS, École Polytechnique, CEA, Sorbonne Université, Institut Polytechnique de Paris, F-91128 Palaiseau Cedex, France

[3]Université Bordeaux-CNRS-CEA, CELIA, UMR5107, 33405 Talence, France

[4]Plasma Physik/PHELIX, GSI Helmholtzzentrum für Schwerionenforschung GmbH, 64291 Darmstadt, Germany

[5]CLPU (Centro de Láseres Pulsados), Edificio M5, Parque Científico USAL, C/Adaja, 8, 37185 Villamayor, Salamanca, Spain

[6]CEA, DAM, DIF, F-91297 Arpajon, France

[7]Université Paris-Saclay, CEA, LMCE, 91680 Bruyères-le-Châtel, France

(Received 29 September 2023; revised 19 March 2024; accepted 20 March 2024)

Laser-driven ion acceleration is well established using solid targets mainly in the target normal sheath acceleration regime. To follow the increasing repetition rate available on high-intensity lasers, the use of high-density gas targets has been explored in the past decade. When interacting with targets reaching densities close to the critical one, the laser pulse can trigger different acceleration mechanisms such as Collisionless Shock Acceleration (CSA) or hole boring. Particle-in-cell simulations using ideal target profiles show that CSA can accelerate a collimated, narrow energy spread and few hundreds of megaelectronvolts ion beam on the laser axis. Nevertheless, in real experiments, the laser will not only interact with an overcritical, thin plasma slab with sharp density gradients, but also with lower density regions surrounding the core of the gas jet, extending to several hundreds of micrometres. The interaction of the laser with these lower density wings will lead to nonlinear effects that will reduce the available energy to drive the shock in the high-density region of the target. Optically tailoring this target could mitigate that issue. Recent experiments conducted on different laser facilities aimed at testing several tailoring configurations. We first tested a scheme with a copropagating picosecond prepulse to create a lower density plasma channel to facilitate the propagation of the main pulse, while the second one was a transverse tailoring driven by nanosecond laser pulses to generate blast waves and form a high-density plasma slab. The main results will be presented here and the methods compared.

Key words: intense particle beams, plasma diagnostics

† Email addresses for correspondence: maitrall@cenbg.in2p3.fr, medhi.tarisien@u-bordeaux.fr

1. Introduction

High intensity laser-driven ion acceleration has been studied for more than two decades and nowadays short proton bunches of up to tens of megaelectronvolts with 10^{12} particle/sr/shot and divergences of the order of several degrees are measured (Snavely *et al.* 2000; Steinke *et al.* 2020). These properties are obtained when the acceleration mechanism at play is Target Normal Sheath Acceleration (TNSA) (Passoni, Bertagna & Zani 2010) where an ultra-high-intensity laser interacts with a solid target. It creates a hot electron population that leaves the target generating fields capable of extracting ions from the surface of the target to accelerate them. Nevertheless using solid targets requires precise alignment at each shot and leads to the generation of debris and the coating of surrounding high-intensity laser optics rendering it delicate to use on the new high repetition rate ultra-high-intensity laser facilities such as Apollon (Papadopoulos *et al.* 2016), ELI (Margarone *et al.* 2018; Radier *et al.* 2022) or VEGA (Huault *et al.* 2017).

To mitigate this issue, self-regenerating targets are under study: comprising of water jets (George *et al.* 2019; Puyuelo-Valdes *et al.* 2022) or droplets (Karsch *et al.* 2003; Ter-Avetisyan *et al.* 2008), cryogenic ribbons (Margarone *et al.* 2016) or liquid crystal films (Thoss *et al.* 2003; Poole *et al.* 2014). Near-critical density targets such as high-density gas jets (Palmer *et al.* 2011; Haberberger *et al.* 2012; Henares *et al.* 2019), potentially cryogenically cooled (Obst *et al.* 2017; Rehwald *et al.* 2023) are also under investigation. Using such targets enables other acceleration mechanisms to participate in the particle energisation. Among the regimes unlocked in this configuration are Magnetic Vortex Acceleration (Bulanov *et al.* 2005; Nakamura *et al.* 2010; Helle *et al.* 2016) or Collisionless Shock Acceleration (CSA) (Silva *et al.* 2004; Fiuza *et al.* 2013; Wan *et al.* 2019). In the latter, the laser pulse generates an electrostatic shock leading to the formation of an interface between two plasma slabs of significantly different densities. This shock propagates colinearly with the laser axis in the plasma at the speed $v_{sh} = MC_s$ where M is its Mach number and C_s the ion acoustic velocity. Above a certain critical Mach number, this shock is able to accelerate ions up to twice its speed. In these idealised simulations, the target is a thin near-critical density slab with very sharp density gradients. This acceleration process can also be studied using pre-expanded foils (Gauthier *et al.* 2014; Pak *et al.* 2018; Tochitsky *et al.* 2020). Coulomb explosion has also been reported as the responsible mechanism for ion acceleration in underdense targets (Krushelnick *et al.* 1999; Sarkisov *et al.* 1999) as well as in the near-critical regime (Wei *et al.* 2004). Here, some electrons, heated by the laser pulse, escape the target volume and leave a space charge force behind them responsible for ion energisation. Using near-critical density gas targets, the hole boring acceleration mechanism can also participate in the acceleration of ions. Here, the radiation pressure associated with the laser pulse is intense enough to push an overdense layer inwards towards the target and accelerate the particles within (Wilks *et al.* 1992; Pukhov & Meyer-ter Vehn 1997).

The main drawback associated with high density gas jets available nowadays comes from the need to obtain a thin layer ($\approx$10s of μm) of near-critical density ($\approx 10^{21}$ e cm^{-3} for 1 μm laser wavelength) at the centre of the target that is positioned in vacuum. Practically, current nozzle designs do not enable the production of a target displaying these ideal characteristics. In fact relatively long (100s of μm), low density ($\approx 10^{19}$ e cm^{-3}) regions are obtained in which the laser has to propagate before reaching the centre of the target and driving the shock (Henares *et al.* 2019) in a region that can be thicker than the optimal value for ion acceleration. The density profile obtained with such targets is presented in figure 1(*a*), where the solid blue line corresponds to experimental data and the dashed red line represents the result of a Computational Fluid Dynamics (CFD) simulation. It

https://doi.org/10.1017/S0022377824000461 Published online by Cambridge University Press

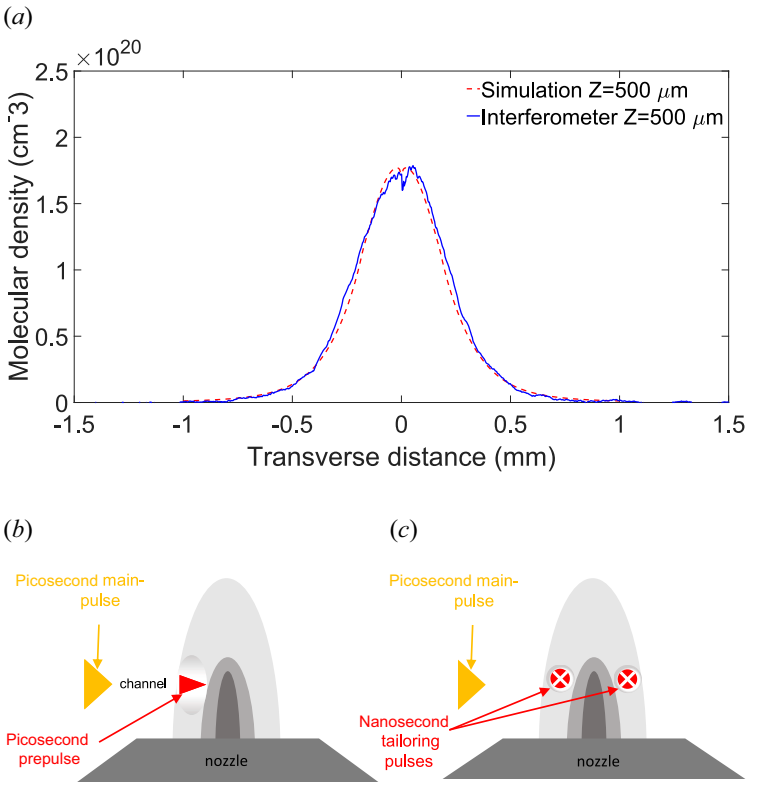

FIGURE 1. Density profile 500 μm from the nozzle fed with 100 bar backing pressure of N_2 exit retrieved with an interferometry set up (solid blue line) or with CFD simulations (red dashed line) (*a*). Figure extracted from Henares *et al.* (2019). Schematic side-view of the laser arrangement in the longitudinal (*b*) and transverse tailoring (*c*) studies, respectively.

is worth noting that there is no adjusting parameter to ensure the very good agreement observed between these two profiles. Moreover, changing the backing pressure will only result in increasing the density overall and will not modify the shape of the profile.

When interacting with a high intensity laser pulse, initially the nanosecond Amplified Spontaneous Emission (ASE) part of the pulse propagates in the target and modifies the initial plasma density profile through optical tailoring. Then, during the propagation in the underdense region of this modified target, the laser undergoes nonlinear effects such as filamentation, loses its integrity and part of its energy, and hence drives a shock that is not as intense nor necessarily in the forward direction of the laser pulse. Consequently, the properties of the accelerated particles are modified, as was shown by Puyuelo-Valdes *et al.* (2019).

Precisely tuning the ASE of a laser chain is challenging, hence optically tailoring the gas target with additional, dedicated prepulses can help improve the control over the obtained density profile and optimise the interaction. This has been experimentally studied with CO_2 lasers ($\lambda_L = 10$ μm) by Tresca *et al.* (2015) and Dover *et al.* (2016) with a copropagating laser pulse to create the sharpest gradient, hence driving the most efficient shock to accelerate ions. Promising results were also obtained earlier by Haberberger *et al.* (2012) with a train of pulses sent to a near-critical density target with the same laser

https://doi.org/10.1017/S0022377824000461 Published online by Cambridge University Press

wavelength. More recently another scheme was discussed in the 1 μm laser wavelength regime with tailored laser pulses propagating transversely to the driving laser pulse (Bonvalet *et al.* 2021; Marquès *et al.* 2021). In this scheme the two laser pulses will drive blast waves in front and behind the gas target (with respect to the main laser propagation axis) that will heat and compress the initial density profile to form a sharp gradient, thin plasma slab. The present collaboration led recent experimental campaigns on 1 μm laser facilities where the copropagating scheme, that will be called longitudinal, and the transverse technique were studied. Both schemes are schematically illustrated in figures 1(*b*) and 1(*c*), respectively. A publication focused on a more detailed study on the results obtained in the transverse tailoring configuration was published very recently (Marquès *et al.* 2024).

In this manuscript, the experimental set-up associated with both campaigns will be described and the main results will be presented. Finally, comparisons will be made between the two schemes and conclusions will be drawn.

2. Experimental set-up

2.1. *Longitudinal tailoring*

This study was conducted at GSI with the Petawatt High-Energy Laser for heavy Ion eXperiments (PHELIX) (Bagnoud *et al.* 2010). The prepulse and the main pulse were issued from the same front end, hence had the same characteristics, as follows: the wavelength was 1054 nm with a pulse duration of 500 fs and a contrast of 10^{11} 80 ps before and 10^{10} 100 ps after the main pulse. It was focused in the target chamber by an $f/1.7$ off-axis parabola down to a focal spot size of 5.3 μm full width at half maximum (FWHM) with ≈40 % of the energy contained in the central spot. The root-mean-square (r.m.s.) transverse pointing fluctuation was of the order of 15 % of the FWHM focal spot size in both directions. For ion acceleration studies, the delay between the two pulses was scanned between 10 ps and 1 ns while the energy in the prepulse was varied from 0.1 to 50 J. This results in intensities delivered by the prepulse as high as 6.9×10^{19} W cm^{-2}. The energy in the main pulse was varied from 50 to 100 J corresponding to intensities up to 1.5×10^{20} W cm^{-2}. The r.m.s. energy fluctuation was 10 %. These two spatially overlapping beams are represented in red and orange in figure 2.

The pulses were focused on a high-density gas jet target previously described by Henares *et al.* (2019) made of a supersonic de Laval nozzle showing an exit diameter of 240 μm, fed by a pressure of up to 1000 bar of hydrogen. The target was precisely aligned thanks to side-view and bottom-view optical diagnostics not depicted in figure 2. The interaction could be probed thanks to a pick off of the beams subsequently frequency doubled to 526 nm and propagating through the target. This 500 fs probe beam could be delayed thanks to a motorised delay stage positioned in the chamber. This beam is depicted in green in figure 2. A shadowgraphy and Nomarski interferometry set-ups were developed to diagnose the generated plasma at different interaction times. These diagnostics were protected with a series of filters including strong bandpass filters (FB530-10 from Thorlabs).

Three Magnetic Spectrometer (MS, represented in black in figure 2) coupled to image plate (IP) were used to detect the accelerated protons. They were positioned at 0°, 38° and 90° from the target with respect to the laser axis. They were shielded with lead to increase the signal-to-noise ratio and equipped with pinholes to improve the energy resolution (at distances of 51.5, 165 and 7.5 cm from the interaction point corresponding to 0.15, 0.03 and 1.4 μsr acceptance solid angle, respectively). The energy resolution of these MS was 0.5 % at 1 MeV and 1.2 % at 6 MeV at 0 and 90° and 2 % at 1 MeV and 6 % at 6 MeV

https://doi.org/10.1017/S0022377824000461 Published online by Cambridge University Press

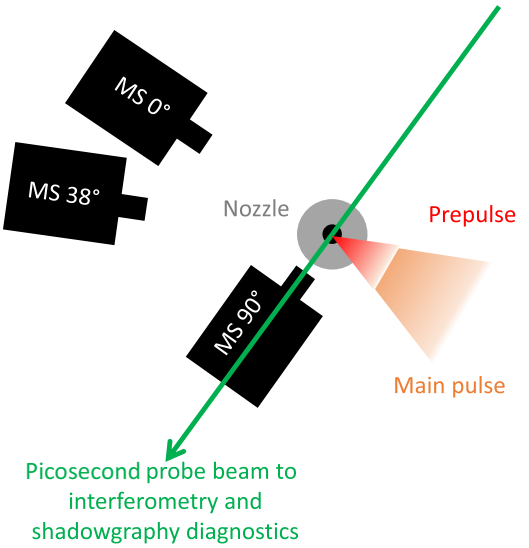

FIGURE 2. Schematic top-view of the experimental set-up implemented for the longitudinal tailoring study. In red/orange the prepulse and main beam are displayed (respectively) while the probe beam path is in green and the three magnetic spectrometers (MS) deployed are indicated in black. The 90° MS is located below the probe beam path. The schematic is not to scale.

at 38°. The BAS-MS IPs from the Fuji Photo-Film Co. Ltd were used and analysed with a FUJIFILM FLA-7000 reader. The IP response function to protons has been taken from Bonnet *et al.* (2013).

2.2. *Transverse tailoring*

The study on transverse tailoring discussed in the present manuscript took place at the LULI laboratory (Ecole Polytechnique, France) on the PICO2000 laser. In this experiment the tailoring pulses propagated transversely compared with the driving pulse. The latter had a wavelength of 1054 nm, a pulse duration of 1 ps and a contrast of 10^9 80 ps before and 100 ps after the main pulse. It was focused by an off-axis parabola to a focal spot size of 10 μm FWHM (displayed in orange in figure 3). The energy in this pulse was varied from 40 to 60 J resulting in an intensity as high as 2×10^{19} W cm^{-2}. The tailoring pulses were also at a wavelength of 1054 nm but presented a duration of 0.6 ns and were focused thanks to a lens down to 42 μm FHWM. The energy in each arm varied from 4 to 6 J. The focal spots positions for all beams varied by $\pm \sim 20$ μm over the experimental run. These two tailoring beams are colinear and represented in red in figure 3.

The target used is similar to the one presented in the previous section. The probe beam came from a seeded Nd:YAG laser source which delivers 7 ns pulses at 532 nm (Quanta-Ray LAB-150). This beam is depicted in green in figure 3. The optical diagnostics used in this experiment consisted of a shadowgraphy set-up with a CCD camera coupled to a gated optical intensifier (GOI) recording two-dimensional spatially resolved snap shots and a streak camera to monitor the time evolution along the picosecond axis.

Similarly to the previous set-up, two MS with IPs were used to detect the accelerated protons (represented in black in figure 3). They were positioned at 0° and 30° from the target with respect to the laser axis (at distances of 55 and 45 cm from the interaction point corresponding to 0.65 and 0.97 μsr acceptance solid angle, respectively). The energy

https://doi.org/10.1017/S0022377824000461 Published online by Cambridge University Press

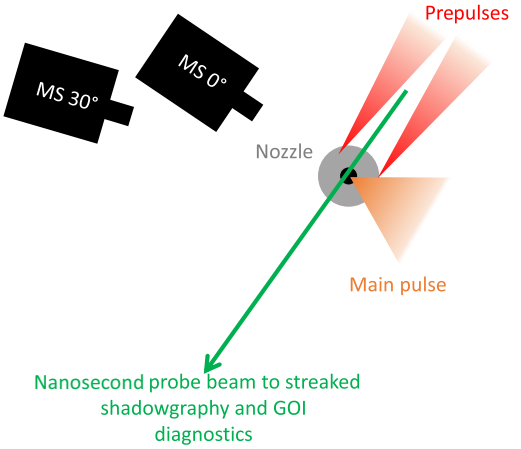

FIGURE 3. Schematic top-view of the experimental set-up implemented for the transverse tailoring study. In orange the main beam path is displayed while the nanosecond tailoring beam path is in red prior to the target, the probe beam is in green and the two MS deployed are indicated in black. The schematic is not to scale.

resolution of these MS was 0.2 % at 1 MeV. The same acquisition and analysis procedures have been applied as described in the previous section.

3. Experimental results

3.1. *Longitudinal tailoring*

3.1.1. *Plasma target tailoring study*

Initially, studies were conducted to investigate the formation of a plasma channel at low laser energy and low hydrogen backing pressures. Thanks to the interferometry diagnostic, it was revealed that a lower density plasma channel is formed, as can be seen in figure 4(*a*). This image results from firing a 5 J laser pulse corresponding to an intensity of 5.8×10^{18} W cm^{-2} on 100 bar hydrogen backing pressure target probed 312 ps after the interaction. On this image the laser propagates from left to right and its focusing geometry is depicted by the red cone. The nozzle is placed on top, not shown on the image. The fringes' curvature appears to change twice around the laser axis (vertically on the image), which is a signature of a lower density region. Analysing this image to obtain the plasma density is challenging but focusing on a region where the fringes are relatively symmetric around the laser axis, $Z = -300$ μm and $Y = -200$ μm depicted as region A in figure 4(*a*), allows us to estimate the value of the density. This is what is depicted in figure 4(*b*) where the solid blue line is the density profile obtained along the white dashed line in figure 4(*a*) and the red dashed line is the results of a CFD simulation without a tailoring pulse. In this area (edges of the plasma channel), the analysis showed an increase of the density by a factor ∼2.5 compared with the expected density from the unperturbed gas jet obtained from CFD simulations. Assuming that this density has been pushed by the laser pulse away from the laser axis, where the plasma channel is formed (region B in figure 4*a*), this means that at this delay the electronic density in the plasma channel is lower than without plasma tailoring.

For laser–plasma interaction at higher backing pressures, radiation will be emitted at twice the initial frequency of the laser pulse in the regions where it interacts with a high plasma density and sharp gradient. This is the bright emission region that can be seen in figure 5. The figure shows images recorded on the shadowgraphy diagnostic with

https://doi.org/10.1017/S0022377824000461 Published online by Cambridge University Press

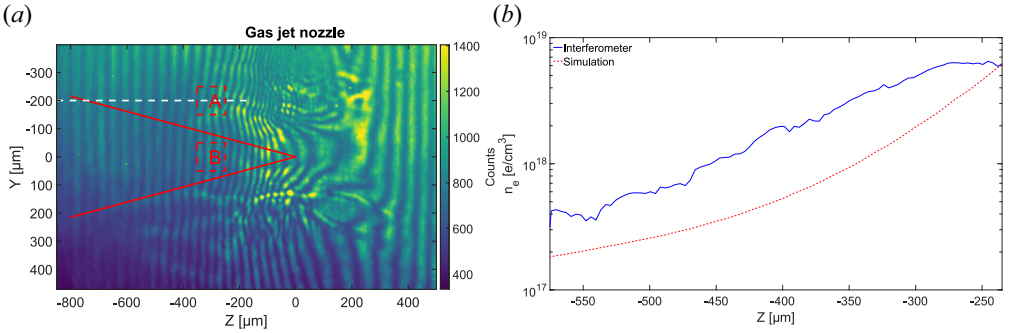

FIGURE 4. Raw interferogram of the target firing at 100 bar hydrogen backing pressure 312 ps after the interaction with a 5 J laser pulse corresponding to an intensity of 5.8×10^{18} W cm^{-2}. The nozzle is on top of the image (not shown) and the laser propagates from left to right (*a*). The 0 graduations on the longitudinal (Z) and height (Y) axis mark where the laser is focused. The focusing laser is indicated by the red cone. The letters A and B correspond to regions that will be referred to in the core of the text. The white dashed line is where the density profile is reconstructed and shown in (*b*) with a solid blue line. The dashed red line in (*b*) corresponds to CFD simulation results without a tailoring pulse.

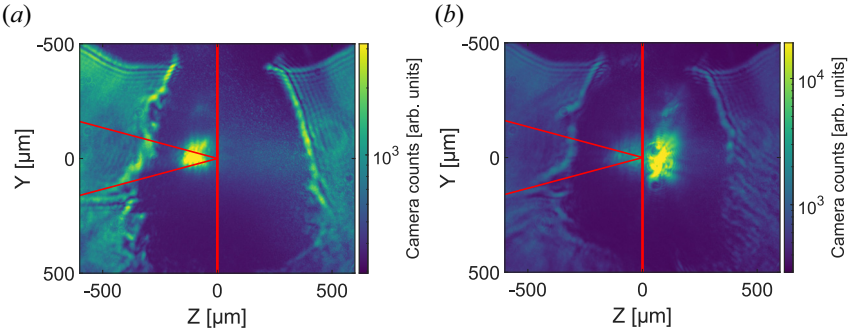

FIGURE 5. Shadowgraphy images obtained after the interaction of a laser pulse with a gas jet fed by a 800 bar hydrogen backing pressure. The probe beam is sent 312 ps after the interaction with the main pulse. The focusing laser pulse is depicted with a red cone while the vertical line represents the centre of the nozzle. Here (*a*) is obtained without a prepulse and with a main pulse intensity of a 5.8×10^{18} W cm^{-2} while (*b*) is with a 1 J prepulse (1.5×10^{18} W cm^{-2}) sent 300 ps before the main pulse for which the intensity was 4.5×10^{18} W cm^{-2}.

the nozzle on top and the focusing laser represented by the red cone. The vertical line represents the centre of the nozzle where the density is the highest. For both these shots the backing pressure was fixed at 800 bar of hydrogen and the probing time was 312 ps after the interaction with the main pulse. Figure 5(*a*) is obtained without prepulse and with 5 J in the main pulse (5.6×10^{18} W cm^{-2}) while figure 5(*b*) is with a 1 J prepulse (1.5×10^{18} W cm^{-2}) sent 300 ps before the 4 J main pulse (4.5×10^{18} W cm^{-2}). The dark region below the trapezoidal nozzle shape corresponds to a region significantly larger than the volume where the density is above the critical density for the 532 nm probe pulse wavelength because of its refraction in the density gradients. This is described in detail in Marquès *et al.* (2024). It is clear that with the prepulse, the frequency-doubled radiation is emitted after the centre of the gas jet (≈100 μm) while without it is emitted ≈100 μm prior to the centre. Measuring the 2ω radiation being emitted from after the centre of the

https://doi.org/10.1017/S0022377824000461 Published online by Cambridge University Press

nozzle indicated that the laser propagated farther inside the high-density part of the target and delivered its energy in this region, which was in good agreement with the initial goal.

3.1.2. *Particle acceleration*

Since the previous section showed the formation of a plasma channel that enabled the laser pulse to deposit its energy farther inside the gas target, the next step was to look at the effect of this optical tailoring on the particle acceleration thanks to the three MS installed.

To do so the laser energy of the main pulse was increased up to 100 J (corresponding to an intensity of 1.5×10^{20} W cm^{-2}) and the hydrogen backing pressure to 1000 bar. The energy contained in the prepulse was varied between 0.1 and 1 J (corresponding to intensities of 1.5×10^{17} W cm^{-2} and 1.5×10^{18} W cm^{-2}, respectively) and the delay between the prepulse and the main pulse was tuned between 10 and 1000 ps. A reference shot without prepulse was also recorded for comparison. The results are presented in figure 6 where figure 6(*a–c*) correspond to the data obtained with a 0.1 J prepulse on the different MS and figure 6(*d–f*) to the series obtained with a 1 J prepulse. The rows correspond to the MS at 0° (figure 6*a*,*d*), 38° (figure 6*b*,*e*) and 90° (figure 6*d*,*f*), respectively. The different solid lines correspond to the distinct prepulse delays used while the dashed lines represent the detection limits.

At 0° both the number of accelerated particles and the maximum energy obtained reduce when adding a prepulse in the delay range explored similarly with a 0.1 or 1 J prepulse (see figures 6*a* and 6*d*). It seems to follow a trend where the longer the delay, the less protons are accelerated at lower energies. The effect is stronger at higher prepulse energy.

At 38° structures appear at relatively low delay (10 to 100 ps) with energy peaks of 6 MeV but tend to vanish at larger delays for both prepulse energy. There are two clear structures at a delay of 10 ps with a 0.1 J prepulse at ≈3.5 and ≈6 MeV persisting at 100 ps delay (figure 6*b*). While for the 1 J case a structure (at ≈2.5 MeV) can only be seen for a 100 ps delay (figure 6*e*).

At 90°, no clear structures can be observed in the range between 1 and 6 MeV. The proton signal detected at 1 J prepulse energy and 10 ps delay is very perturbed and requires more work to be presented. Moreover, the energy limit is set at 6 MeV on these spectra because the spectrometer was positioned much closer to the interaction point (∼7 cm) than to the other two (>50 cm), leading to a very large x ray spot on the IP during some shots. The result was a very high level of background noise, similar in intensity to the proton signal, which renders the estimation of the proton number challenging above 6 MeV. Nevertheless, in the configuration where a 0.1 J prepulse was fired 100 ps before the main pulse, we were able to observe a structure around ≈7.5 MeV clearly separated from the background, as shown in the raw IP presented in figure 7.

The observed structures at different angles cannot be attributed to TNSA or Coulomb explosion. The latter is most likely responsible for the acceleration of the low energy, continuous proton distribution on axis and at the other angles as the shape and maximum energy observed are compatible with the results reported in Krushelnick *et al.* (1999) and Sarkisov *et al.* (1999). In fact, the maximum energy is the relativistic ponderomotive energy $U_p = m_e c^2(\gamma - 1)$ where $\gamma = (1 + a_0^2/2)^{(1/2)}$ is the Lorentz factor for the electron transverse motion. Given the a_0 (normalised laser intensity) of the main pulse reached during that experiment, it corresponds to ≈3 MeV which is in good agreement with the measured energy. The observed structures could be the result of shocks driven by the filamenting laser pulse. Among the ion acceleration mechanisms accessible during the interaction of a laser and underdense or near-critical density plasmas, CSA is one of the few that can produce structured spectra. If the prepulse does not generate a plasma channel with a low enough density, because the energy is too small or the delay too

https://doi.org/10.1017/S0022377824000461 Published online by Cambridge University Press

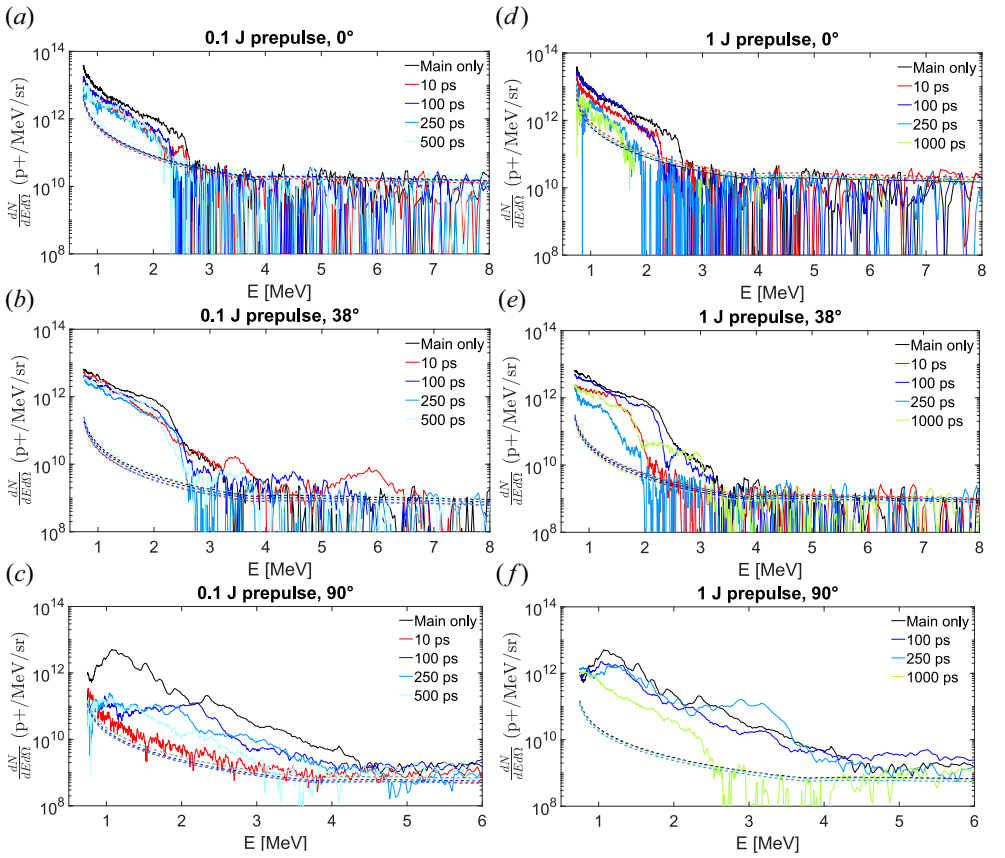

FIGURE 6. Series of spectra obtained during the prepulse energy and delay scans. Panels (*a–c*) corresponds to 0.1 J energy in the prepulse while the second one (*d*)–(*f*) corresponds to 1 J energy (intensities of 1.5×10^{17} W cm^{-2} and 1.5×10^{18} W cm^{-2}, respectively). The three rows correspond to the 0° (*a*,*d*), 38° (*b*,*e*) and 90° (*c*,*f*) MS, respectively. The different spectra in the same graphic, shown in different colours, correspond to distinct delays between the prepulse and the arrival of the main pulse. The black solid line indicated the shot without the prepulse. The detection limit is calculated with the noise specific to each shot and indicated by dashed lines.

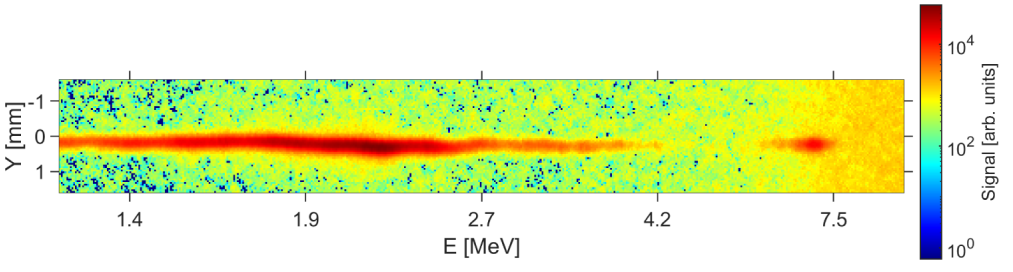

FIGURE 7. Raw image of an IP positioned in the 90° MS after a 0.1 J prepulse was fired 100 ps before the main pulse at 1000 bar backing pressure. A clear structure can be observed ≈ 7.5 MeV.

https://doi.org/10.1017/S0022377824000461 Published online by Cambridge University Press

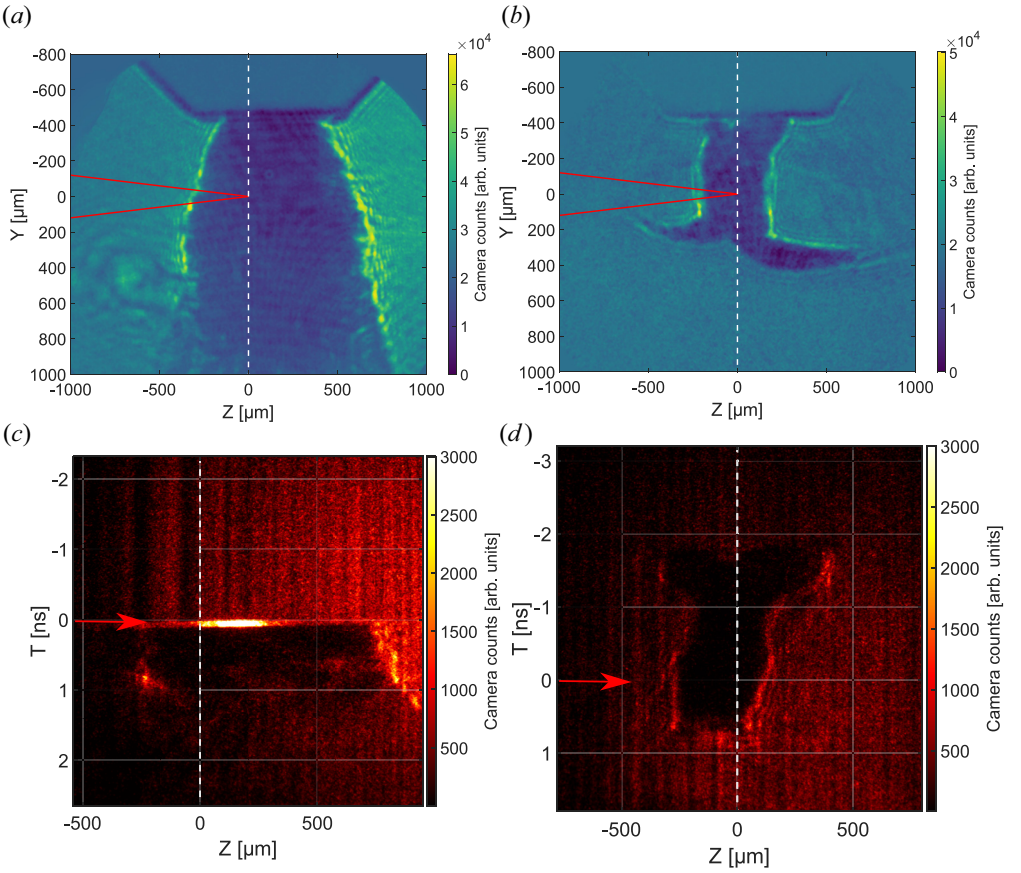

FIGURE 8. (*a*) Shadowgraphy data obtained after the interaction of a 1.2×10^{19} W cm^{-2} laser pulse with a gas jet fed by a 800 bar hydrogen backing pressure. (*b*) Similar data obtained at 200 bar backing pressure with two 3×10^{14} W cm^{-2} tailoring pulses sent 2.4 ns before the main pulse. The diagnostic was triggered 200 ps or 100 ps before the arrival of the main pulse, respectively, and in both cases exposed for 100 ps. The focusing laser pulse is depicted with a red cone while the vertical line represents the centre of the nozzle. (*c*,*d*) Corresponding laser shots on the streak camera where the main laser pulse arrival time is indicated by a red arrow.

short for example, the main laser pulse could still filament and drive shocks in various directions leading to the observations of structures in the spectra at distinct angles and for different delays. It is worth noting that no clear structures could be observed without a prepulse. This could be explained because a clear shock cannot easily propagate in the current experimental conditions without tailoring.

3.2. *Transverse tailoring*

3.2.1. *Plasma target tailoring study*

A reference shot was taken without tailoring pulses at 800 bar backing pressure with a main pulse intensity of 2×10^{19} W cm^{-2} with the GOI triggered 200 ps after the arrival of the main pulse, exposed for 100 ps and the shadowgraphy image associated with this shot is shown in figure 8(*a*). As in figure 5, the nozzle is on top of the figure and the focusing laser is depicted by the red cone. Similarly to the previous section, the dark region is significantly larger than the actual transverse size of the volume where the density is

https://doi.org/10.1017/S0022377824000461 Published online by Cambridge University Press

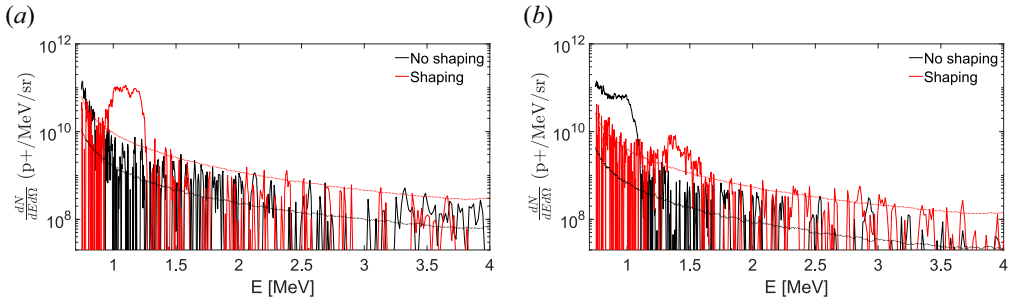

FIGURE 9. Proton spectra obtained at 0° (*a*) and 30° (*b*) from the laser axis with (red solid line) and without (black solid line) the tailoring pulses as described in figure 8. The detection limit is calculated with the noise specific to each shot and indicated by dashed lines.

above the critical one. Figure 8(*b*) was obtained with two tailoring pulses arriving 2.4 ns before the main pulse with a 200 bar backing pressure and the GOI triggered 100 ps before the arrival of the main pulse and exposed for 100 ps. In that case, blast waves propagate towards the centre of the target and create a dense plasma slab in the centre where the driving laser is focused. The associated streak camera images are shown in figures 8(*c*) and 8(*d*) where the main laser pulse arrival time is indicated by a red arrow.

Using the streak camera diagnostic, without the prepulses, it can be noticed that the main pulse creates almost instantaneously a 1 mm-wide plasma (figure 8*c*). With the tailoring beams (figure 8*d*), the propagation of the two blast waves can be diagnosed temporally until they collide and form the transient target. One can note that, on this shot, the main pulse arrives after the thinnest target size was obtained.

3.2.2. *Particle acceleration*

The spectra obtained on the magnetic spectrometers at 0° and 30° for the two shots described in the previous section are represented in figures 9(*a*) and 9(*b*), respectively. A continuous distribution is obtained with a maximum energy lower than 1.5 MeV at both angles without tailoring (black solid lines). With the tailoring pulses, structures are observed in the distributions around 1–1.5 MeV. These structures are a signature of a different acceleration mechanism compared with the case without tailoring. When the target is not optically modified, the spectrum obtained resembled the ones obtained from the Coulomb explosion mechanism with a characteristic continuous distribution at various angles. When tailoring the target, quasimonoenergetic structures appear that could be the result of CSA due to the presence of sharper gradients enabled by the tailoring of the target. It can also be noted that, overall, fewer protons are produced at 30° rendering the acceleration process more directional as expected from CSA and more protons are accelerated to relatively high energy with plasma tailoring.

4. Discussions

Several challenges were identified during the experimental campaigns where high-density gas targets were used. First, due to the density profiles obtained with the nozzles available nowadays, optical tailoring strategies must be implemented experimentally to reduce the low-density wings and have thin, near-critical density targets. This optical tailoring is challenging to precisely diagnose in three dimensions as optical probing results in two-dimensional reconstruction that can be misleading. Furthermore, the beam time constraints and repetition rate on such laser facilities also limits the

https://doi.org/10.1017/S0022377824000461 Published online by Cambridge University Press

parameter phase space that can be explored in these multibeam experiments (energy and duration of the pulses, Rayleigh lengths, delays, wavelength, . . .). One can also note that spatially extended particle diagnostics could improve the obtained data as the angles at which the particles are accelerated are difficult to predict and could vary shot-to-shot. Target tailoring, as well as the shot-to-shot variation of the laser pulse focal spot, which are reasonably small in the presented work, could lead to a modification of the symmetry of the target, hence ions could be emitted at angles that are not covered by the particle detectors with the limited acceptance angle used here.

Nevertheless, a clear effect of the optical tailoring of the high-density gas jet targets on the particle spectra obtained has been demonstrated in both configurations. In the longitudinal one, the first observations seem to indicate that a plasma channel can be formed, enabling the laser pulse to propagate and deposit its energy farther towards the centre of the target. However, within the performed parameters scan, this does not result in the acceleration of higher energy protons in the forward direction, as could be expected. Still, clear structures could be observed up to energies of 6 MeV at 38° and 90° only when the target was optically tailored. This could be a signature of the laser pulse propagating to a higher density but still undergoing filamentation and generating shocks at various angles. During this experiment, the explored phase space was limited especially in terms of prepulse energy and delay between the pulses and future experiments are required to extend this phase space. It could also be noted that the profile at the rear of the target was not tailored in this scheme as opposed to the transverse one, which is not ideal for CSA to occur according to the particle-in-cell simulations presented by Fiuza *et al.* (2013).

The transverse scheme is more complicated to set up as it requires the synchronisation and spatial alignment of several beams from distinct sources but showed promising results as clear structures were obtained in the forward direction. It is worth noting that this scheme facilitates working at much lower backing pressure which is in favour of using it at higher repetition rate. Nevertheless, the explored phase space was again limited.

To conclude, even though a clear effect associated with the plasma tailoring was measured, leading to the observation of structures in the spectrum at several megaelectronvolts of energy, each of the presented spectra were obtained from a single shot. To mitigate the potentially biased results and to enable the exploration of broader phase spaces, parametric studies would need to be performed on high repetition rate, high intensity laser facilities. This would enable the exploration of common phase spaces between the two configurations, hence making a direct comparison easier but also unlocking a clear understanding of the mechanisms at play to develop the laser plasma acceleration of ions on near-critical gas targets.

Acknowledgements

Part of the results presented here are based on the experiment P-21-00004, which was performed at the PHELIX facility at the GSI Helmholtzzentrum für Schwerionenforschung, Darmstadt (Germany). The authors would like to give special thanks to the PHELIX operation team as well as the staff of the LULI facility.

Editor V. Malka thanks the referees for their advice in evaluating this article.

Declaration of interest

The authors report no conflict of interest.

https://doi.org/10.1017/S0022377824000461 Published online by Cambridge University Press

Funding

This work is supported by IN2P3-CNRS (nos. 2016-2024 ALP-IONS projects); Agence Nationale de la Recherche (ANR-17-CE30- 0026-Pinnacle); the Region Nouvelle Aquitaine (AAPR2022-2021-17029010 VALERIA); LASERLAB-EUROPE (grant agreement no. 871124, European Union's Horizon 2020 research and innovation programme) and the authors acknowledge the financial support of the IdEx University of Bordeaux / Grand Research Program 'GPR LIGHT'.

Data availability

The data that support the findings of this study are available from the corresponding authors, A.M. or M.T., upon reasonable request.

REFERENCES

BAGNOUD, V., *et al.* 2010 Commissioning and early experiments of the PHELIX facility. *Appl. Phys.* B **100** (1), 137–150.

BONNET, T., COMET, M., DENIS-PETIT, D., GOBET, F., HANNACHI, F., TARISIEN, M., VERSTEEGEN, M. & ALEONARD, M.M. 2013 Response functions of Fuji imaging plates to monoenergetic protons in the energy range 0.6–3.2 MeV. *Rev. Sci. Instrum.* **84** (1), 013508.

BONVALET, J., *et al.* 2021 Laser-driven collisionless shock acceleration of protons from gas jets tailored by one or two nanosecond beams. *Phys. Plasmas* **28** (11), 113102.

BULANOV, S.V., DYLOV, D.V., ESIRKEPOV, T.Z., KAMENETS, F.F. & SOKOLOV, D.V. 2005 Ion acceleration in a dipole vortex in a laser plasma corona. *Plasma Phys. Rep*. **31** (5), 369–381.

DOVER, N.P., COOK, N., TRESCA, O., ETTLINGER, O., MAHARJAN, C., POLYANSKIY, M.N., SHKOLNIKOV, P., POGORELSKY, I. & NAJMUDIN, Z. 2016 Optical shaping of gas targets for laser–plasma ion sources. *J. Plasma Phys*. **82** (1).

FIUZA, F., STOCKEM, A., BOELLA, E., FONSECA, R.A., SILVA, L.O., HABERBERGER, D., TOCHITSKY, S., MORI, W.B. & JOSHI, C. 2013 Ion acceleration from laser-driven electrostatic shocks. *Phys. Plasmas* **20** (5), 056304.

GAUTHIER, M., *et al.* 2014 Investigation of longitudinal proton acceleration in exploded targets irradiated by intense short-pulse laser. *Phys. Plasmas* **21** (1), 013102.

GEORGE, K.M., *et al.* 2019 High-repetition-rate (kHz) targets and optics from liquid microjets for high-intensity laser–plasma interactions. *High Power Laser Sci. Engng* **7**, e50.

HABERBERGER, D., TOCHITSKY, S., FIUZA, F., GONG, C., FONSECA, R.A., SILVA, L.O., MORI, W.B. & JOSHI, C. 2012 Collisionless shocks in laser-produced plasma generate monoenergetic high-energy proton beams. *Nat. Phys*. **8** (1), 95–99.

HELLE, M., GORDON, D., KAGANOVICH, D., CHEN, Y., PALASTRO, J. & TING, A. 2016 Laser-accelerated ions from a shock-compressed gas foil. *Phys. Rev. Lett*. **117** (16), 165001.

HENARES, J.L., *et al.* 2019 Development of gas jet targets for laser-plasma experiments at near-critical density. *Rev. Sci. Instrum*. **90** (6), 063302.

HUAULT, M., *et al.* 2017 Commissioning experiments of VEGA-2 at Centro de Láseres Pulsados (CLPU). In *Frontiers in Optics 2017 (2017), paper FM2B.4*, p. FM2B.4. Optica Publishing Group.

KARSCH, S., DÜSTERER, S., SCHWOERER, H., EWALD, F., HABS, D., HEGELICH, M., PRETZLER, G., PUKHOV, A., WITTE, K. & SAUERBREY, R. 2003 High-intensity laser induced ion acceleration from heavy-water droplets. *Phys. Rev. Lett*. **91** (1), 015001.

KRUSHELNICK, K., *et al.* 1999 Multi-MeV ion production from high-intensity laser interactions with underdense plasmas. *Phys. Rev. Lett*. **83** (4), 737–740.

MARGARONE, D., *et al.* 2016 Proton acceleration driven by a nanosecond laser from a cryogenic thin solid-hydrogen ribbon. *Phys. Rev.* X **6** (4), 041030.

MARGARONE, D., *et al.* 2018 ELIMAIA: a laser-driven ion accelerator for multidisciplinary applications. *Quant. Beam Sci*. **2** (2), 8.

MARQUÈS, J.R., *et al.* 2021 Over-critical sharp-gradient plasma slab produced by the collision of laser-induced blast-waves in a gas jet: application to high-energy proton acceleration. *Phys. Plasmas* **28** (2), 023103.

MARQUÈS, J.R., *et al.* 2024 Collisionless shock acceleration of protons in a plasma slab produced in a gas jet by the collision of two laser-driven hydrodynamic shockwaves. *Matt. Radiat. Extremes* **9** (2).

NAKAMURA, T., BULANOV, S.V., ESIRKEPOV, T.Z. & KANDO, M. 2010 High-energy ions from near-critical density plasmas via magnetic vortex acceleration. *Phys. Rev. Lett*. **105** (13), 135002.

OBST, L., *et al.* 2017 Efficient laser-driven proton acceleration from cylindrical and planar cryogenic hydrogen jets. *Sci. Rep*. **7** (1), 10248.

PAK, A., *et al.* 2018 Collisionless shock acceleration of narrow energy spread ion beams from mixed species plasmas using 1 μm lasers. *Phys. Rev. Accel. Beams* **21** (10), 103401.

PALMER, C.A.J., *et al.* 2011 Monoenergetic proton beams accelerated by a radiation pressure driven shock. *Phys. Rev. Lett*. **106** (1), 014801.

PAPADOPOULOS, D.N., *et al.* 2016 The Apollon 10 PW laser: experimental and theoretical investigation of the temporal characteristics. *High Power Laser Sci. Engng* **4**, e34.

PASSONI, M., BERTAGNA, L. & ZANI, A. 2010 Target normal sheath acceleration: theory, comparison with experiments and future perspectives. *New J. Phys*. **12** (4), 045012.

POOLE, P.L., ANDERECK, C.D., SCHUMACHER, D.W., DASKALOVA, R.L., FEISTER, S., GEORGE, K.M., WILLIS, C., AKLI, K.U. & CHOWDHURY, E.A. 2014 Liquid crystal films as on-demand, variable (50-5000 nm) targets for intense lasers. *Phys. Plasmas* **21** (6), 063109.

PUKHOV, A. & MEYER-TER VEHN, J. 1997 Laser hole boring into overdense plasma and relativistic electron currents for fast ignition of ICF targets. *Phys. Rev. Lett*. **79** (14), 2686–2689.

PUYUELO-VALDES, P., *et al.* 2019 Proton acceleration by collisionless shocks using a supersonic H2 gas-jet target and high-power infrared laser pulses. *Phys. Plasmas* **26** (12), 123109.

PUYUELO-VALDES, P., *et al.* 2022 Implementation of a thin, flat water target capable of high-repetition-rate MeV-range proton acceleration in a high-power laser at the CLPU. *Plasma Phys. Control. Fusion* **64** (5), 054003.

RADIER, C., *et al.* 2022 10 PW peak power femtosecond laser pulses at ELI-NP. *High Power Laser Sci. Engng* **10**, e21.

REHWALD, M., *et al.* 2023 Ultra-short pulse laser acceleration of protons to 80 MeV from cryogenic hydrogen jets tailored to near-critical density. *Nat. Commun*. **14** (1), 4009.

SARKISOV, G.S., BYCHENKOV, V.Y., NOVIKOV, V.N., TIKHONCHUK, V.T., MAKSIMCHUK, A., CHEN, S.Y., WAGNER, R., MOUROU, G. & UMSTADTER, D. 1999 Self-focusing, channel formation, and high-energy ion generation in interaction of an intense short laser pulse with a He jet. *Phys. Rev.* E **59** (6), 7042–7054.

SILVA, L.O., MARTI, M., DAVIES, J.R., FONSECA, R.A., REN, C., TSUNG, F.S. & MORI, W.B. 2004 Proton shock acceleration in laser-plasma interactions. *Phys. Rev. Lett*. **92** (1), 015002.

SNAVELY, R.A., *et al.* 2000 Intense high-energy proton beams from petawatt-laser irradiation of solids. *Phys. Rev. Lett*. **85** (14), 2945–2948.

STEINKE, S., *et al.* 2020 Acceleration of high charge ion beams with achromatic divergence by petawatt laser pulses. *Phys. Rev. Accel. Beams* **23** (2), 021302.

TER-AVETISYAN, S., SCHNÜRER, M., NICKLES, P.V., SMIRNOV, M.B., SANDNER, W., ANDREEV, A., PLATONOV, K., PSIKAL, J. & TIKHONCHUK, V. 2008 Laser proton acceleration in a water spray target. *Phys. Plasmas* **15** (8), 083106.

THOSS, A., RICHARDSON, M., KORN, G., FAUBEL, M., STIEL, H., VOGT, U. & ELSAESSER, T. 2003 Kilohertz sources of hard x rays and fast ions with femtosecond laser plasmas. *JOSA* B **20** (1), 224–228.

TOCHITSKY, S., PAK, A., FIUZA, F., HABERBERGER, D., LEMOS, N., LINK, A., FROULA, D.H. & JOSHI, C. 2020 Laser-driven collisionless shock acceleration of ions from near-critical plasmas. *Phys. Plasmas* **27** (8), 083102.

TRESCA, O., DOVER, N., COOK, N., MAHARJAN, C., POLYANSKIY, M., NAJMUDIN, Z., SHKOLNIKOV, P. & POGORELSKY, I. 2015 Spectral modification of shock accelerated ions using a hydrodynamically shaped gas target. *Phys. Rev. Lett*. **115** (9), 094802.

https://doi.org/10.1017/S0022377824000461 Published online by Cambridge University Press

WAN, Y., ANDRIYASH, I., HUA, J., PAI, C.H., LU, W., MORI, W., JOSHI, C. & MALKA, V. 2019 Two-stage laser acceleration of high quality protons using a tailored density plasma. *Phys. Rev. Accel. Beams* **22** (2), 021301.

WEI, M.S., *et al.* 2004 Ion acceleration by collisionless shocks in high-intensity-laser–underdense-plasma interaction. *Phys. Rev. Lett*. **93** (15), 155003.

WILKS, S.C., KRUER, W.L., TABAK, M. & LANGDON, A.B. 1992 Absorption of ultra-intense laser pulses. *Phys. Rev. Lett*. **69** (9), 1383–1386.

https://doi.org/10.1017/S0022377824000461 Published online by Cambridge University Press